Resistivity structure around the focal area of the 2004 Rumoi-Nanbu earthquake (*M* 6.1), northern Hokkaido, Japan

Hiroshi Ichihara[1]*, Ryo Honda[1], Toru Mogi[1], Hideaki Hase[1], Hiroyuki Kamiyama[2], Yusuke Yamaya[1], and Yasuo Ogawa[3]

[1]*Institute of Seismology and Volcanology, Hokkaido University, N10W8 Kita-ku, Sapporo, Japan*
[2]*Ueyama-Shisui Co. Ltd., 1-7, N2E13, Higashi-ku, Sapporo, Japan*
[3]*Volcanic Fluid Research Center, Tokyo Institute of Technology, 2-12-1 Ookayama, Meguro-ku, Tokyo, Japan*

(Received March 2, 2007; Revised April 10, 2008; Accepted May 14, 2008; Online published September 8, 2008)

The Rumoi-Nanbu earthquake (*M* 6.1) occurred in northern Hokkaido, Japan, on December 14, 2004. We conducted MT surveys along three profiles in and around the focal area to delineate and decipher the structural features of the seismogenic zone. The inverted 2-D resistivity images of the three sections comprised two layers: an upper conductive layer and a lower resistive layer. The boundary of these layers lay at a depth of approximately 3–5 km. A comparison with the surface geology and drilling data revealed that the upper conductive layer and the lower resistive layer corresponded to the Cretaceous–Tertiary sedimentary rocks and older basement rocks, respectively. A clear upheaval of the layer boundary was found along the profile at the center of the focal area. In addition, borehole data indicated an obvious increase in the Young's modulus toward the lower layer. Therefore, the elastic properties with a complex geometry around the focal zone tended to vary; this probably depicts the zone of stress accumulation that triggered the earthquake.

Key words: Magnetotellurics, stress concentration, intraplate earthquake, northern Hokkaido.

1. Introduction

Strain accumulation zones with a large convergence of 20 mm/year, such as the Niigata-Kobe Tectonic Zone (NKTZ) (Sagiya *et al*., 2000), have been reported by the Japanese nationwide GPS array (GEONET). The localized strain concentrations possibly resulted from heterogeneities in the crust under the tectonic stress (Iio *et al*., 2002, 2004). A number of quaternary active faults have been reported, and large earthquakes have been occurring (e.g., 2004 Mid-Niigata prefecture earthquake (*M* 6.8)) around the strain concentration zones. Therefore, a delineation of the structural heterogeneities underneath the strain concentration zone plays an important role in understanding the occurrence of intraplate earthquakes. The Rumoi-Nanbu earthquake (*M* 6.1) occurred in northern Hokkaido, Japan, on December 14, 2004. The focal mechanism of this earthquake was a reverse fault type. The strike direction was almost north to south (N-S). The focal area was under the east to west (E-W) compression at the eastern margin of the Japan Sea (Takahashi *et al*., 1999). The Geographical Survey Institute (1997) also revealed a clear east-west contracting strain concentration around the focal area. The correspondence between the focal mechanism and the strain concentration resembled the earthquakes in the NKTZ. Therefore, the imaging of the crustal structure can provide fundamental information on the earthquake mechanism and processes.

The electrical resistivity in the crust is mainly controlled by the existence of pore fluid and its connectivity (e.g., Archie, 1942; Unsworth *et al*., 1997). Thus, low resistivity zones at subsolidus temperatures are often interpreted as porous zones with fluid. For example, the observed low resistivity images along the faults could be explained as the existence of an abundant quantity of fluid in cracks or fault breccias (e.g., Unsworth *et al*., 1997; Hoffmann-Rothe *et al*., 2004). Recent magnetotelluric (MT) investigations have also revealed low resistivity zones distributed in the mid to lower crust beneath the intraplate earthquake zones (e.g., Mitsuhata *et al*., 2001; Ogawa *et al*., 2001; Ogawa and Honkura, 2004; Wannamaker *et al*., 2004; Uyeshima *et al*., 2005; Yoshimura *et al*., 2008). Those low resistivity zones are interpreted as fluid reservoirs from which the fluid is supplied, triggering the intraplate earthquake in the upper layer (e.g., Iio *et al*., 2002). However, a resistivity image does not only reflect the porosity or the presence of the fluid but also provides information regarding in situ temperature or lithology. Thus, the resistivity boundaries often represent geological boundaries (e.g., Park and Wernicke, 2003).

In this study, we conducted wide-band MT surveys and analyzed the electrical resistivity images of the focal area. To delineate the structural variation along a geological trend, we imaged a two-dimensional (2-D) resistivity section along three profiles in the E-W direction. The resistivity structure was carefully interpreted by integrating the geophysical and geological structures and petro-physical properties from well-log data with the aim of determining

*Now at Earthquake Research Institute, the University of Tokyo, 1-1-1, Yayoi, Bunkyo-ku, Tokyo.

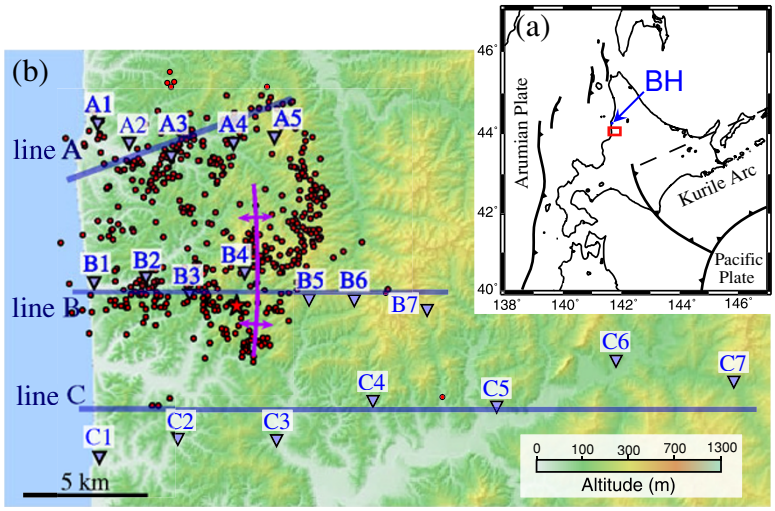

Fig. 1. (a) Tectonic framework around Hokkaido and survey area (red rectangle). "BH" denotes the location of the borehole drilled by the Japan National Oil Corporation (1986). (b) Locations of MT sites are indicated with blue inverted triangles. Red star and circles denote relocated mainshock and aftershocks, respectively (Ichiyanagi *et al*., 2007). A purple line indicates an anticline axis revealed by Tsushima *et al*. (1956) and our investigation.

the probable relationship between subsurface structure and the occurrence of earthquakes.

2. MT Survey and Data Processing

We conducted MT surveys along three profiles (Fig. 1) in June and August 2006. Lines A and B were set across the aftershock area, while line C was set outside it. Line B passes over the epicenter of the mainshock. The time series of MT data were recorded using MTU-2000 system (Phoenix Geophysics Ltd.). Magnetic fields were measured with three orthogonal induction coils. Electric fields were measured with orthogonal dipoles attached to Pb-$PbCl_2$ electrodes on both sides. The recorded time series data were converted into a frequency-domain impedance tensor using the cascade decimation technique developed by Wight and Bostick (1980). The converted frequency ranged between 320 and 0.00034 Hz. We applied a remote reference technique (Gamble *et al*., 1979) to avoid bias due to the existence of local magnetic noise. The referenced data was the horizontal magnetic field data of the Esashi station, approximately 500 km from the Rumoi area, operated by the Geographical Survey Institute. Consequently, high-quality data were obtained, except that for the frequency range between 1 and 0.1 Hz (dead band) at a few sites along line A.

3. Two-dimensional Resistivity Structure

3.1 Estimation of 2-D strike direction

We applied site- and frequency-dependent Groom-Bailey (referred to as G-B hereafter) decomposition (Groom and Bailey, 1989) to evaluate strike azimuths. In a frequency range of 320 to 0.01 Hz, dominant strike azimuths are N-S (or E-W) at line B and C (Fig. 2). In contrast, the dominant azimuth is N25°W-S25°E (or N65°E-S65°W) along line A. For the lower frequency band (0.01–0.00034 Hz), dominant strikes were determined at N45°W-S45°E or N45°E-S45°W along all the lines. Induction vectors in the frequency range between 1 and 0.01 Hz were dominantly oriented westward (Fig. 2), corresponding to the direction of the sea. However, the length of the induction vector at site B3 was larger

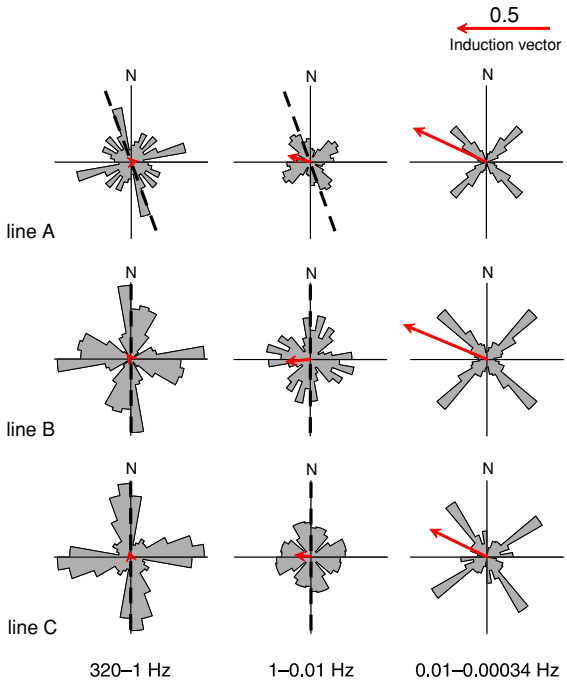

Fig. 2. Strike estimates from Groom-Bailey decompositions wherein distortion parameters are set as site- and frequency-dependent. Averaged induction vectors are denoted by red solid arrows. Thick dashed lines denote strike directions adopted in the 2-D analysis.

than that at site B2, although site B2 was located nearer to the sea than site B3. The difference in the lengths in the frequency range of 2 to 0.00034 Hz exceeded 0.1; this indicated that the induction vectors were affected not only by an ocean effect but also by structures beneath the inland region. On the other hand, the dominant direction of the induction vector in the lower frequency band (<0.01 Hz) was N70°W. The induction vector exhibited no dominant direction and had a small length (approximately <0.05) in the frequency range of 320 to 1 Hz. A phase tensor analysis (Caldwell *et al*., 2004) did not indicate evidence for

strong three-dimensionality in the higher frequency band (320–0.01 Hz); it did exhibit a weak variation of max azimuth and a small skew angle ($\beta < 3^\circ$) in all the survey lines (not shown in figure). However, data in the lower frequency band (0.01–0.00034 Hz) clearly revealed a strike oriented in the N50°W-S50°E direction and a high skew angle ($3^\circ < \beta < 25^\circ$) in most of the MT sites; this implied a strong three-dimensionality. Because the strike directions estimated from the G-B decomposition and induction vectors were not fixed and rotated with frequency variation in the lower frequency band (0.01–0.00034 Hz), the data in the lower frequency band obviously included a 3-D effect. The high skew angle observed in the phase tensor analysis also suggested a structural three-dimensionality in the lower frequency band. Therefore, we excluded the lower frequency band (<0.01 Hz) for 2-D inversion. The result of G-B decomposition shows the N-S or E-W strike azimuth for lines B and C. The induction vectors indicate the N-S strike azimuth in their possibilities. Thus, we assumed an N-S direction for the 2-D strikes along lines B and C. The N-S strikes were consistent with the coastline, regional geological boundaries, and strikes of the outcropped sedimentary rocks (Tsushima *et al.*, 1956, 1958). The focal plane axis of the 2004 earthquake also extended along the same direction (Ichiyanagi *et al.*, 2007). However, the phase tensor analyses does not show specific max azimuth, possibly indicating that horizontal resistivity variation is not significant. The strike direction for line A was set to N20°E-S20°W, subject to the result of the G-B decomposition. This direction was inconsistent with that of the induction vector and differed from that of the estimated strikes of the other lines, implying that a three-dimensionality in the structure was strong around line A as compared to the other profiles.

3.2 Two-dimensional inversion and the result

The projections of apparent resistivity and phase in transverse electric (TE) and transverse magnetic (TM) modes were inverted by using a 2-D inversion code developed by Ogawa and Uchida (1996) wherein the static shift of both modes is estimated as a parameter. The impedances used for the inversion were not rectified via the Groom-Bailey decomposition because the variation in the twists and shears with frequency for each site was insignificant (<10°). The inversion started with a 10 Ohm-m homogeneous half-space model with a fixed resistivity of the seawater (0.3 Ohm-m) during iterations. An error floor of 10% in apparent resistivity and an equivalent in phase are applied in each inversion. The observed impedances were mostly explained on an inverted model (Fig. 3). The root mean square (RMS) errors for lines A, B, and C in the initial models (7.43, 6.94, and 5.04, respectively) were reduced to 1.49, 1.05, and 0.79, respectively, via the inversion procedure. The final inverted resistivity models are shown in Fig. 4. All models are typically composed of two layers: a shallower conductive (0.3–10 Ohm-m) layer extending from the surface down to a depth of approximately 4 km and an underlying resistive (10–300 Ohm-m) layer. A significant feature of our model along line B is the heterogeneity above the mainshock. The resistivity beneath site B4 at a depth of 3 km was 20 Ohm-m, while the resistivity of the surrounding blocks at an equivalent depth was 5–10 Ohm-m, indicating an upheaval area of the lower resistive layer above the southern region of the earthquake. The location of the anticline observed in surface geology (Figs. 1, 4) corresponded to this structure. On the other hand, no such structure was observed along line A, line C, or the along-strike extension of the anticline along line B. A detailed discussion on this feature has been provided in the preceding sections. The resistivity below 6 km in all sections was 30–300 Ohm-m, which appeared to be homogeneous. Heterogeneities in the lower resistive layer, however, were hardly detected by the MT data due to the existence of the thick upper conductive layer.

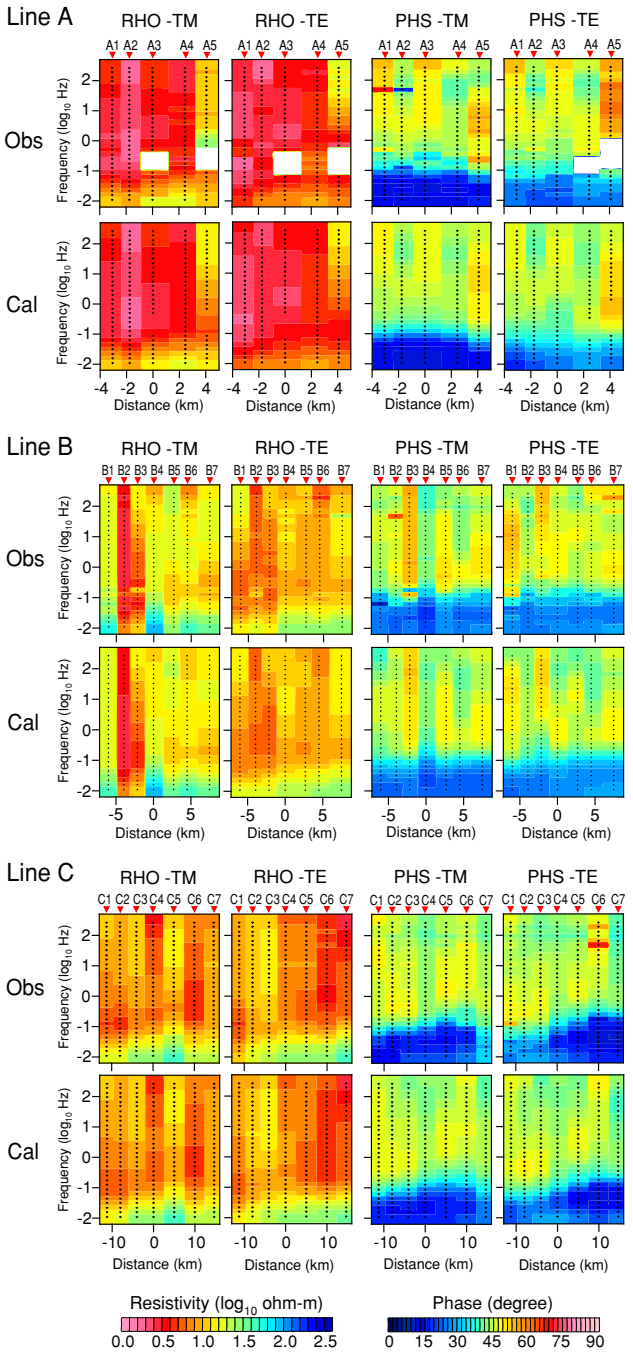

Fig. 3. Pseudo-sections of observed data and calculated response in the final model for TM and TE mode data. Apparent resistivity and phase are labeled with RHO and PHS, respectively.

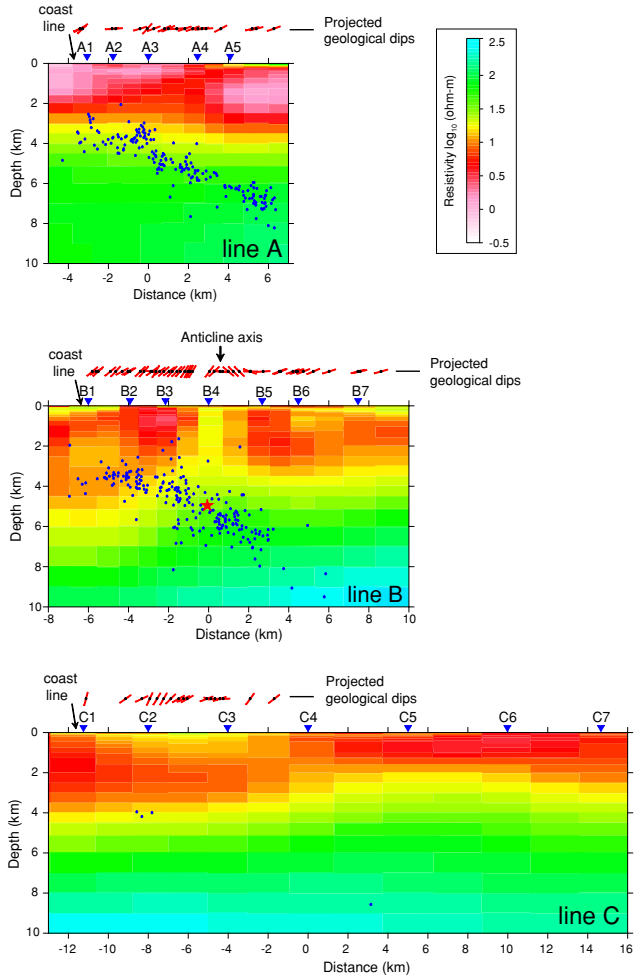

Fig. 4. Inverted resistivity models for lines A, B, and C for TE and TM mode impedance. Blue dots denote aftershocks (Ichiyanagi *et al.*, 2007) along 2.0 km wide profile. Geological dips (Tsushima *et al.*, 1956, 1958; this investigation) projected to profiles are shown above profiles.

4. Discussion

4.1 Effect of sea water

Although the presence of seawater near but still outside of the profiles may affect the MT data, the inverted models are still reliable. One reason for this is that the model is validated by the inversion test with a hypothetical model described in Ogawa (2002) and Takakura (2004). The hypothetical model includes a near surface conductor outside of the profile. The inversion test with TE + TM mode reasonably recovered the hypothetical model. Another reason is that the seawater slightly affects the MT data in our research area. The resistivity contrast between the seawater (0.3 Ohm-m) and the uppermost layer beneath our profiles (0.3–10 Ohm-m) is small. In addition, the seafloor is shallower than 100 m within 30 km of the coastline. The induction vectors also indicate an insignificant seawater effect because of their small lengths in the high-frequency band (>0.03 Hz). However, the induction vectors in the lower frequency band lower than 0.03 Hz are oriented toward the coastline.

4.2 Interpretation of resistivity structure

The deep borehole data (Japan National Oil Corporation, 1986) obtained 9 km north from MT site A2 (Fig. 1) was used for verifying the inverted result and for interpretations. The borehole data revealed sedimentary rocks from the Tertiary and Cretaceous (0–4675 m) and andesites from the earlier Cretaceous–Jurassic (from 4675 m to the bottom of this borehole (5023 m)). The logged resistivity of the upper sedimentary rocks and lower igneous rocks were 3–50 Ohm-m and 15–500 Ohm-m, respectively. This vertical resistivity variation was consistent with our inverted resistivity images. Therefore, the upper conductive layer and the lower resistive layer of the inverted images correspond to the sedimentary rocks and the basement igneous rocks, respectively. A previous MT study by Ogawa *et al.* (1992) also supports our inverted result. Ogawa *et al.* (1992) settled an approximately 100 km length of the wide-band MT survey line oriented E-W direction in approximately 10 km north of line A. They modeled a conductive layer (less than 30 Ohm-m) at the near surface (0.5–3 km in depth) and a deep conductor (30 Ohm-m, >20 km in depth). A resistive zone (>100 Ohm-m) fills between the conductors. Their result is consistent with our result at the near surface (>5 km in depth). Thus, the resistivity feature in the present study consisting of upper conductive layer and lower resistive layer seems to be extended northward. Their model also verifies the interpretation of resistivity structure based on the borehole data (Japan National Oil Corporation, 1986) because the borehole is located in the profile by Ogawa *et al.* (1992). However, the deep conductor by Ogawa *et al.* (1992) is not clarified in our inverted images because lower frequency data (<0.01 Hz) were not inverted. In order to clarify the deep conductor, 3-D modeling, which enables us to use the lower frequency data, will be done in a future study.

4.3 Validity test for a protruded resistivity zone

In the vicinity of site B4 along line B, a protrusion in the lower resistive layer interrupts the upper conductive layer. The splitting of the apparent resistivity between the TM and TE modes at site B4 (Fig. 5) indicates a structural variation in the horizontal direction and supports the protruded resistive zone. In addition, a variation in the TM phase between sites B3 and B5 (Fig. 3) indicates a 2-D heterogeneity along

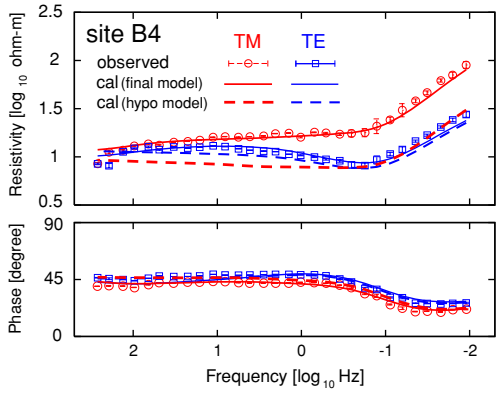

Fig. 5. Observed and calculated sounding curves for apparent resistivity and phase of site B4 along line B. Circles indicate observed TM mode apparent resistivity and phase. Blue solid line and red dotted line are the responses of the inverted model and hypothetical model, respectively. Explanation of hypothetical models is provided in text.

Table 1. Velocity and resistivity logging data and apparent density of borehole drilled 9 km north of site A2 based on Japan National Oil Corporation (1986). Young's modulus calculated assuming that the Poisson ratio is 0.25.

Depth (m)	Lithology	Density (kg/m^3)	V_p (km/s)	Young's module (GPa)	Resistivity (Ohm-m)
0–2450	Miocene	2280±210 ($N = 15$)	3.00	17.1	3– 10
2450–3342	Paleogene	2330±140 ($N = 9$)	3.93	30.0	3– 30
3342–4675	Cretaceous	2480±150 ($N = 13$)	4.44	40.7	7– 50
0–4675	(Average of sediments)	2360±190 ($N = 37$)	3.49	24.0	3– 50
4675–5023	Basement rock	2750± 70 ($N = 4$)	4.77	52.1	15–500

line B. We conducted hypothetical tests to confirm whether the protruded resistive body is required by the observed MT impedances. We tested the model by removing the resistive body under site B4. Specifically, the resistivity value of the parameter blocks at a depth of 0.2–3 km under site B4 was set to 10 Ohm-m. The forward responses on the hypothetical model at site B4 were inconsistent with the impedance in the TM mode (Fig. 5). The calculated apparent resistivity for the hypothetical model in the lower frequency range (<1 Hz) was less than 50% of that of the final model and observed data. The RMS error for the TE and TM mode of the hypothetical model was increased to 1.22 from 1.05 in the final model. In addition, the splitting of the apparent resistivity between the TE and TM modes was explained with the protruded resistive zone.

4.4 Crustal heterogeneity and stress concentration around the focal zone

The protruded resistive zone in the lower resistive layer corresponds to the anticline structure orthogonal to the MT lines (Fig. 1). This is obvious from the spatial distribution of the geological dips (Tsushima *et al.*, 1956). The anticline axis is located just above the undulated zone, as shown in Fig. 4. The width and amplitude of this upheaval along line B are approximately 3 km and 5 km, respectively. The N-S elongated high Bouguer anomaly zone around site B4 (Honda *et al.*, 2007) supports the existence of the anticline structure. The high anomaly indicates the existence of protruded dense basement rocks. The density of the basement rock (2750±70 kg/m^3, Table 1) is significantly larger than that of the sedimentary rocks (2360±190 kg/m^3). The length of the anticline along the axis is probably less than 11 km along the strike direction because the undulated resistive zone is found neither along line A nor along line C (Fig. 4); this implies structural variation along the strike direction and the existence of a 3-D heterogeneity. The Bouguer anomaly and geological structure support the observations. The elongated high gravity anomaly along the anticline is not found along lines A and C. In addition, the dip distribution on the surface geology (Tsushima *et al.*, 1956) also does not reveal a clear anticline along lines A and C (Figs. 1 and 4). The mainshock occurred below the anticline structure. Here, we discuss whether this heterogeneity can cause the initiation of an earthquake. The Japan National Oil Corporation (1986) reported the physical properties of the core samples and borehole logging (Table 1). On the basis of these properties, the Young's modulus of the sedimentary layers and basement rocks were estimated to be 24.0 GPa and 52.1 GPa, respectively; this implies a complex rigidity distribution around the focal area caused by the undulation of the boundary. In general, the heterogeneity of elastic properties under a regional stress field produces a localized stress concentration (e.g., Chatterjee and Mukhopadhyay, 2002). Thus, the heterogeneity due to the anticline probably produces the localized stress concentration. This was a significant cause for the generation of the 2004 Rumoi-Nanbu earthquake. In addition, the 3-D heterogeneity may also affect the stress concentration. Thus, a 3-D analysis will be carried out in the future study. It will also enable us to interpret the impedance in the lower frequency band (<0.01 Hz) and to obtain the resistivity structure at larger depths.

5. Conclusion

We delineated the 2-D resistivity structures in the upper crust around the focal area of the 2004 Rumoi-Nanbu earthquake (M 6.1). All the inverted resistivity images consisted of a subsurface conductive layer and an underlain resistive body, the boundary of which was 3–5 km in depth. Based on the borehole logging data, the subsurface conductive layer and the underlain resistive body were confirmed as Cretaceous–Tertiary sedimentary rocks and older igneous rocks, respectively. The elastic properties of these layers had distinct values. The boundary between those layers was severely undulated just above the mainshock, implying the existence of heterogeneity in the elastic properties around the focal area that induced the strain concentration. The mainshock could have been generated by the localized strain concentration.

Acknowledgments. The Japan National Oil Corporation provided the borehole logging data. The Esashi Observatory of the Geographical Survey Institute provided the continuous MT data used as a remote reference. We thank the landowners for their cooperation in establishing the observation sites. The editor, M. Uyeshima, and two reviewers, T. Goto and the other, anonymous, helped us improve the manuscript. Helpful discussions with Dr. T. Hashimoto, Mr. M. Ichiyanagi, and Dr. H. Takahashi from the Institute of Seismology and Volcanology, Hokkaido University, and Dr. Ch. Sivaji from the Department of Science and Technology, Govt. of India improved the contents of this paper. Some of our figures are drawn with Kashimir (http://www.kashmir3d.com/index.html), GMT (Wessel and Smith, 1998), and Gnuplot (Thomas Williams and Colin Kelley).

References

Archie, G. E., The electrical resistivity log as an aid in determining some reservoir characteristics, *Trans. Am. Inst. Min. Metall. Pet. Eng.*, **146**, 54–62, 1942.

Caldwell, T. G., H. M. Bibby, and C. Brown, The magnetotelluric phase tensor, *Geophys. J. Int.*, **158**, 457–469, 2004.

Chatterjee, R. and M. Mukhopadhyay, Effects of rock mechanical properties on local stress field of the Mahanadi basin, India—results from finite element modeling, *Geophys. Res. Lett.*, **29**, doi:10.1029/2001GL013447, 2002.

Gamble, T. D., J. Clarke, and W. M. Goubau, Magnetotellurics with a remote magnetic reference, *Geophysics*, **44**, 53–68, 1979.

Geographical Survey Institute, *Horizontal strain in the Hokkaido district, Japan*, http://www.gsi.go.jp/, 1997.

Groom, R. W. and R. C. Bailey, Decomposition of magnetotelluric impedance tensors in the presence of local three-dimensional galvanic distortions, *J. Geophys. Res.*, **94**, 1913–1925, 1989.

Hoffmann-Rothe, A., O. Ritter, and C. Janssen, Correlation of electrical conductivity and structural damage at a major strike-slip fault in northern Chile, *J. Geophys. Res.*, **109**, doi:10.1029/2004JB003030, 2004.

Honda, R., H. Kamiyama, T. Yamaguchi, H. Ichihara, and T. Mogi, Gravity survey in and around the focal area of 2004 Rumoi-nanbu earthquake, Northern Hokkaido, Northern Japan, *Geophysical bulletin of Hokkaido Univ.*, **70**, 2007 (in press; in Japanese with English abstract).

Ichiyanagi, M., T. Maeda, T. Yamaguchi, H. Takahashi, M. Kasahara T. Sasatani, and A. Yamamoto, Aftershock distribution of the December 14, 2004 Rumoi-nanbu Earthquake (M 6.1) in the northern part of Hokkaido, Japan, *Zishin 2*, **59**, 209–221, 2007 (in Japanese with English abstract).

Iio, Y., T. Sagiya, Y. Kobayashi, and I. Shiozaki, Water-weakened lower crust and its role in the concentrated deformation in the Japanese Islands, *Earth Planet. Sci. Lett.*, **203**, 245–253, 2002.

Iio, Y., T. Sagiya, and Y. Kobayashi, Origin of the concentrated deformation zone in the Japanese Islands and stress accumulation process of intraplate earthquakes, *Earth Planets Space*, **56**, 831–842, 2004.

Japan National Oil Corp., *Research report on the pilot drilling at "Rumoi" for prospecting petroleum and natural gas in Japan*, 86 pp., 1986 (in Japanese).

Mitsuhata, Y., Y. Ogawa, M. Mishina, T. Kono, T. Yokokura, and T. Uchida, Electromagnetic heterogeneity of the seismogenic region of 1962 M 6.5 Northern Miyagi Earthquake, northeastern Japan, *Geophys. Res. Lett.*, **28**, 4371–4374, 2001.

Ogawa, Y., On two-dimensional modeling of magnetotelluric field data, *Surv. Geophys.*, **23**, 251–272, 2002.

Ogawa, Y. and T. Uchida, A two-dimensional magnetotelluric inversion assuming Gaussian static shift, *Geophys. J. Int.*, **126**, 69–76, 1996.

Ogawa, Y. and Y. Honkura, Mid-crustal electrical conductors and their correlations to seismicity and deformation at Itoigawa-Shizuoka tectonic line, central Japan, *Earth Planets Space*, **56**, 1285–1291, 2004.

Ogawa, Y., Y. Nishida, M. Uyeshima, Y. Mitsuhata, M. Makino, and Y. Nakayama, Deep crustal structures in Hokkaido, Japan, derived from wide-band magnetotelluric method, *Monthly Chikyu*, **14**, 545–550, 1992 (in Japanese).

Ogawa, Y., M. Mishina, T. Goto, H. Satoh, N. Oshiman, T. Kasaya, Y. Takahashi, T. Nisitani, S. Sakanaka, M. Uyeshima, Y. Takahashi, Y. Honkura, and M. Matsushima, Magnetotelluric imaging of fluids in intraplate earthquakes zones, NE Japan back arc, *Geophys. Res. Lett.*, **28**, 3741–3744, 2001.

Park, S. K. and B. Wernicke, Electrical conductivity images of Quaternary faults and Tertiary detachments in the California Basin and Range, *Tectonics*, **22**, doi:10.1029/2001TC001324, 2003.

Sagiya, T., S. Miyazaki, and T. Tada, Continuous GPS array and present day crustal deformation of Japan, *Pure Appl. Geophys.*, **157**, 2303–2322, 2000.

Takahashi, H., M. Kasahara, F. Kimata, S. Miura, K. Heki, T. Seno, T. Kato, N. Vasilenko, A. Ivashchenko, V. Bahtiarov, V. Levin, E. Gordeev, F. Korchagin, and M. Gerasimenko, Velocity field of around the Sea of Okhotsk and Sea of Japan regions determined from a new continuous GPS network data, *Geophys. Res. Lett.*, **26**, 2533–2536, 1999.

Takakura, S., Precise investigation and interpretation of subsurface resistivity structure by high-density measurement of electrical and electromagnetic methods, Ph.D. thesis, Kyoto University, 348 pp., 2004 (in Japanese).

Tsushima, K., K. Matsuo, and S. Yamaguchi, *Geological map of Japan*, "Onishika" with explanatory text, 1–17, 1956 (in Japanese with English abstract).

Tsushima, K., K. Tanaka, K. Matsuo, and S. Yamaguchi, *Geological map of Japan*, "Tappu" with explanatory text, 1–66, 1958 (in Japanese with English abstract).

Unsworth, M. J., P. E. Malin, G. D. Egbert, and J. R. Booker, Internal structure of the San Andreas fault at Parkfield, California, *Geology*, **25**, 359–362, 1997.

Uyeshima, M., Y. Ogawa, Y. Honkura, S. Koyama, N. Ujihara, T. Mogi, Y. Yamaya, M. Harada, S. Yamaguchi, I. Shiozaki, T. Noguchi, Y. Kuwaba, Y. Tanaka, Y. Mochido, N. Manabe, M. Nishihara, M. Saka, and M. Serizawa, Resistivity imaging across the source region of the 2004 Mid-Niigata Prefecture earthquake (M 6.8), central Japan, *Earth Planets Space*, **57**, 441–446, 2005.

Wannamaker, P. E., T. G. Caldwell, W. M. Doerner, and G. R. Jiracek, Fault zone fluids and seismicity in compressional and extensional environments inferred from electrical conductivity: the New Zealand Southern Alps and U. S. Great Basin, *Earth Planets Space*, **56**, 1171–1176, 2004.

Wessel, P. and W. H. F. Smith, New, improved version of the Generic Mapping Tools released, *EOS Trans. AGU*, **79**, 579, 1998.

Wight, D. E. and F. X. Bostick, Cascade decimation—a technique for real time estimation of power spectra, in *Proceedings of the IEEE International Conference on Accoustic, Speech Signal Processing*, 626–629, 1980.

Yoshimura, R., N. Oshiman, M. Uyeshima, Y. Ogawa, M. Mishina, H. Toh, S. Sakanaka, H. Ichihara, I. Shiozaki, T. Ogawa, T. Miura, S. Koyama, Y. Fujita, K. Nishimura, Y. Takagi, M. Imai, R. Honda, S. Yabe, S. Nagaoka, M. Tada, and T. Mogi, Magnetotelluric observations around the focal region of the 2007 Noto Hanto Earthquake (M_j 6.9), Central Japan, *Earth Planets Space*, **60**, 117–122, 2008.

H. Ichihara (e-mail: h-ichi@eri.u-tokyo.ac.jp), R. Honda, T. Mogi, H. Hase, H. Kamiyama, Y. Yamaya, and Y. Ogawa